# Evolution of the North American Landscape: New Insights from Biostratigraphy, Geomorphology and Thermochronology

[1]Victoria M. Fernandes, [1]Gareth G. Roberts, [2]Nicky J. White, and [1]Alexander C. Whittaker
v.fernandes17@imperial.ac.uk

Imperial College London

AGU100 ADVANCING EARTH AND SPACE SCIENCE

T41D-0328

## Key Points

(1) North American Cenozoic uplift and denudation from stratigraphy and drainage inversion.

(2) Calibrated landscape evolution model indicates broadly fixed drainage planform and predictable denudation.

(3) Mantle convective support of North America generated Cenozoic uplift.

## 1 Overview

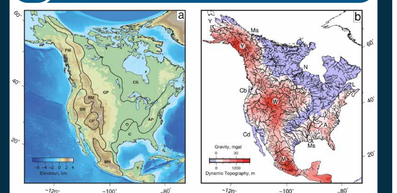

**Figure 1: Topography, drainage and dynamic support of North America.** (a) ETOPO1 topographic dataset and physiographic provinces. (b) Thin black lines = 4161 rivers extracted from ASTER GDEM. Drainage network is shown atop calculated dynamic topography; contours = long wavelength ( < 800 km) free-air gravity anomalies converted to dynamic topography using an admittance, Z = 25 mGal/km from GRACE dataset.

• The present day topography of the Earth's surface is the result of a complex interactions between deep and surface processes operating on multiple spatial and temporal scales. Therefore constraining histories of vertical motion may contain important clues about geological processes. The admittance between long-wavelength (~ 800–2500 km) free-air gravity anomalies and topography in western North America suggests high elevation regions are at least partially supported by sub-plate processes.

## 2 Constraints on Large Scale Vertical Motions

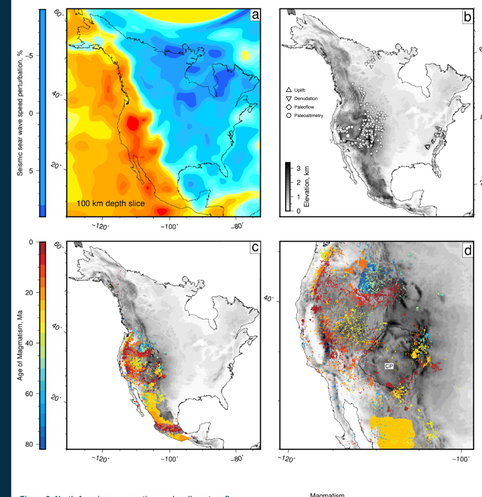

**Figure 3: North American magmatism and sedimentary flux.** Magmatism recorded in the NAVDAT catalog (a) within the Colorado Plateau (b) throughout North America (c) Solid sedimentary flux to the Gulf of Mexico from Galloway et al. (2011), which were calculated using seismic reflection surveys and well data. (d) Uncorrected sedimentary flux calculated from seismic reflection surveys and well data along the New Jersey margin from Poag & Sevon (1989).

**Figure 2:** (a) Shear wave-speed anomaly at 100 km depth (Schaeffer and Lebedev, 2013). (b) Other constraints. (c) Cenozoic magmatism from NAVDAT database (www.navdat.org), orange/yellow polygons = Oligocene/Miocene ignimbrites (d) Western North American magmatism centered on Colorado Plateau.

• The history and chemistry of extrusive western North American magmatism suggest that Cenozoic uplift is related to anomalously warm asthenosphere and decompression melting.

• Correlation of basalt geochemistry with shear wave velocities suggests magmatism and uplift of western North America is generated by modest thermal anomalies beneath a thinned lithosphere

• Trimodal distribution of 6713 samples from the NAVDAT database is broadly coeval with pulses of sedimentary flux to the Gulf of Mexico.

• Other uplift, denudation and paleoaltimetry constraints also point toward a staged uplift history of North America.

## 3 Uplift from Biostratigraphy and Regressive Stratigraphic Sequences

• Dated shoreline deposits and marine fossil assemblages provide locations of known paleo-bathymetry at some time in the past. Therefore the present day elevations of these locations defines a minimum amount of uplift since the time of deposition.

• This cumulative uplift, $\int U \, dt$ , is calculated as the sum of present day elevation $z$, paleo water depth $P$ and paleo-sea level $S$ relative to today. The calculated value is a minimum.

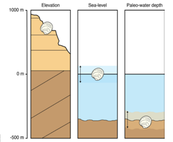

**Figure 5: Schematic diagram illustrating uplift calculation.**

• We compiled an inventory of 4634 unique marine fossil assemblages from the Paleobiology Database (PBDB, https://paleobiodb.org).

• Youngest outcropping marine to terrestrial sedimentary sequences provide additional constraints. Each regressive sequence was identified and datad from the literature and locations extracted from state geological maps (total 339 points).

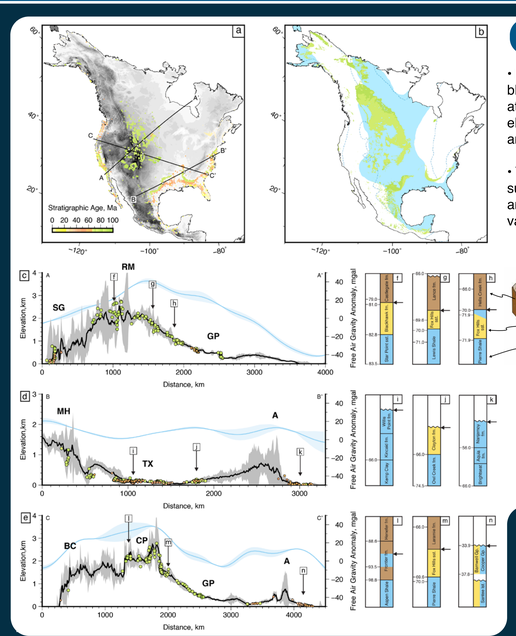

**Figure 4: Biostratigraphic and stratigraphic uplift constraints.** (a) Colored circles show location and age of marine fossil assemblages from PBDB (paleobiodb.org) and youngest outcropping marine to non-marine stratigraphic transitions. Black lines = locations of cross sections; white circles = locations of stratigraphic columns shown in panels (f-h), (i-j) and (l-n). (b) Extent of Late Cretaceous seaway calculated from PBDB compilation. Solid blue polygons/dashed lines = maximum flooding extent of the Cretaceous (Late Maastrichtian) interior seaway from Smith et al. (1994) and Kauffman et al. (1993). Dark/light green polygons = outcropping Lower/Upper Cretaceous rocks. (c-e) Topographic and stratigraphic cross sections; black line/grey band = topography/maximum and minimum elevation within 100 km swath; labeled arrows = location of stratigraphic columns shown in adjacent panels; colored circles = biostratigraphically dated marine rock colored by age. Light blue band = free air gravity anomaly/maximum and minimum within 100 km swath (from GRACE dataset). (f-n) Generalized stratigraphic sections containing youngest marine regression or outcropping marine strata; broadly, blue = shallow marine, yellow = marginal marine/shoreface, brown = terrestrial. Interpreted paleoenvironment shown in schematic diagram.

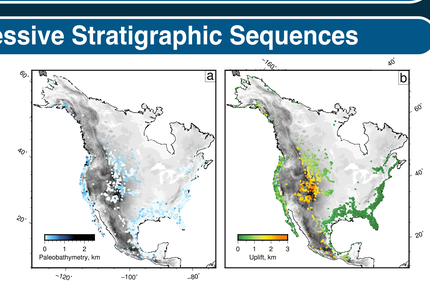

**Figure 6: Interpreted paleo-water depth and uplift from stratigraphic and biostratigraphic constraints.** (a) Paleo-water depth and (b) total uplift for all ages as interpreted from marine to terrestrial transitions and PBDB fossil assemblages.

• Since 80 - 65 Ma a region encompassing the Colorado Plateau, Rocky Mountains and parts of the Great Plains have been uplifted in a broad swell with a wavelength of ~ 1500 km. Measured uplift reaches a maximum of ~ 3 km in the Colorado Plateau and Southern Rocky Mountains and decreases smoothly to ~ 500 m in the eastern Great Plains.

• Long wave length (> 1000 km) post-Cretaceous warping of North American topography and colocated gravity, tomographic and magmatic observations indicate that sub-plate support has played an important role in generating kilometer scale uplift.

## 4 Inverse Modelling of Longitudinal Profiles

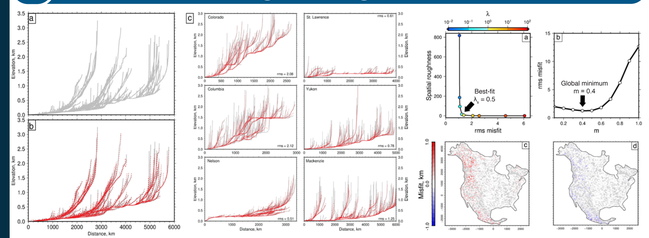

**Figure 7: Inverting drainage patterns for uplift histories: data and best-fitting theory.** (a) Observed longitudinal river profiles of Mississippi and its principal tributaries (rms misfit = 0.47). (b) Observed and calculated river profiles. Gray lines = observed profiles; Red dotted lines = best-fitting profiles calculated by inverse modeling using cumulative uplift history. (c) Observed and calculated longitudinal river profiles of six catchments.In each case, rms misfit is shown (global rms misfit = 1.24).



**Figure 8: Inverse model parametrization.** (a) Data misfit plotted as function of model smoothness for suite of inverse models with different values of smoothing parameter, $\lambda$. (b) Residual misfit plotted as function of erosional parameter m. (c) Positive and (d) Negative misfit map between observed and calculated river profiles.

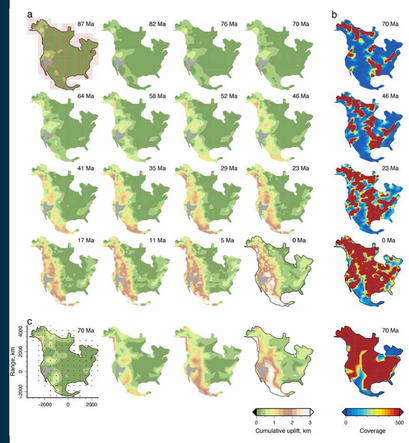

**Figure 9: Calculated cumulative uplift.** (a) North America, calculated by linear inversion of 4161 river profiles (rms misfit = 1.24). Grid of red points in top left-hand panel = loci of spatial vertices used to discretize uplift rate. (b) Selected panels at four different times that show model coverage (i.e. number of non-zero entries in model matrix). (c) Four panels showing cumulative uplift history of North America calculated using coarser mesh (rms misfit = 2.62). (d) Coverage for coarser mesh.

• 4161 drainage profiles were extracted from digital elevation data and their veracity checked using satellite imagery.

• We use a simplified version of the stream power erosional model to linearly invert for a spatially smooth uplift rate history.

$$\frac{\partial z(x,t)}{\partial t} = -vA(x)^m \left( \frac{\partial z(x,t)}{\partial x} \right)^n + U(x,t)$$

• We assume that n = 1, fixed drainage area over space and time, that variable climate does not significantly affect shapes of rivers and diffusive behavior of rivers is unimportant.

• $v$ was calibrated using the incision history recorded by eroded lava dams in the Grand Canyon. The mean incision rate is 111 ± 7 m/Myr, which combined with local slope and area measurements, gives

$$v = 4.16 \times 10^4 \times (2.78 \times 10^{12})^m.$$

• We tested the results of the inverse model by comparing them to uplift measured using our independent biostratigraphic and stratigraphic inventory. We omitted PBDB samples with ages younger than 5 Ma because the temporal resolution of our inverse model is 5.7 Ma.

• 100% and 86% of uplift measurements from stratigraphic and biostratigraphic inventories respectively are matched by the modeled uplift within error within a factor of 2.

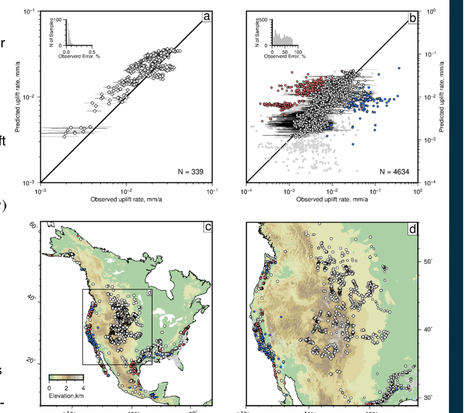

**Figure 10: Tests of results from inverse model.** Comparison of time-averaged Late Cretaceous to Recent uplift from inverse model and independent stratigraphic and biostratigraphic constraints. Solid black line = 1:1 relationship; white/gray points = inverse results similar to stratigraphic estimates; gray points = samples with large (> an order of magnitude) observational uncertainties with error bars omitted for clarity; red/blue points indicate where inverse model over-/under-predicts uplift rate by more than a factor of two. (c) Spatial distribution of stratigraphic and biostratigraphic constraints colored by accuracy of inverse model; symbols same as for panels (a) and (b). (d) Comparison of inversion results and observations centered on Colorado Plateau.

## 5 Landscape Evolution Modelling

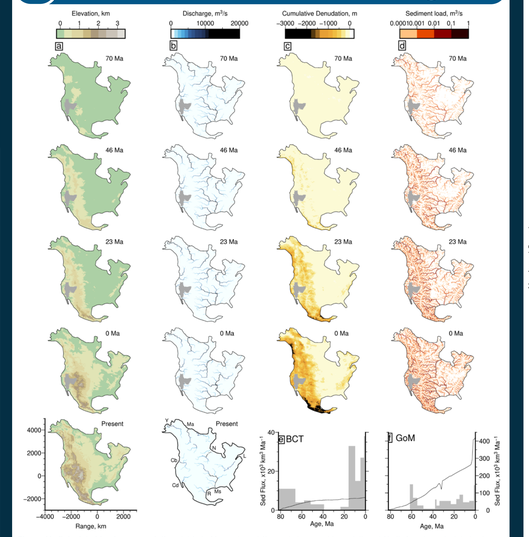

**Figure 11: Calculated landscape evolution.** (a) Late Mesozoic and Cenozoic topographic evolution of North America calculated using a modified version of Badlands landscape evolution model. Model was parameterized using uplift history calculated from calibrated North American river provile inversion. Model resolution = 10 km. Lowest panel = modern topography from ASTER GDEM. (b) Calculated discharge; final panel = modern discharge calculated using Esri flow routing algorithms and ASTER GDEM. (c) Calculated cumulative denudation. (d) Calculated sedimentary load. Calculated solid sedimentary flux (black line) compared to published estimates (grey) for the (e) Baltimore Canyon Trough (Poag & Sevon, 1989) and (f) Gulf of Mexico (Galloway et al., 2011).

• Using the results from our inverse scheme we parametrized a modified version of the Basin and Landscape Dynamics (Badlands) model to predict Mesozoic-Recent topography, discharge, denudation and sedimentary flux.

• We purposefully kept the forward model as simple as possible, using the same erosional parameter values ($v$, $m$, $n$) as in our inverse model. Sea-level was assumed to be constant ($z = 0$) and precipitation rate, $P$, was set to unity. The flexural response to unloading, glacial erosion and ice cover were not included. The resulting model has the form

$$\frac{\partial z}{\partial t} = -v(AP)^m \nabla z - \kappa \nabla^2 z + U(x,y,t)$$

## 6 Thermochronology

• We test our predicted denudation history using the results from two well-known thermochronometers: apatite fission track (AFT) and apatite (U-Th)/He (A-He). Data compiled from 74 papers and existing databases, with 1074 AFT and 323 A-He points.

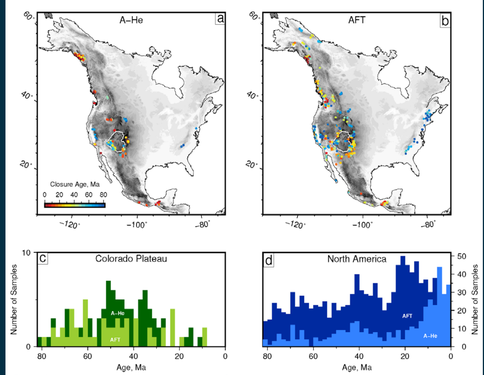

**Figure 12: Low-temperature thermochronology data.** (a) Synthesis of independent estimates of thermochronometric A-He closure ages across North America. Gray shading = modern topography from ETOPO1 database; thin white line encloses Colorado Plateau. (b) AFT closure ages. (c) Histograms of A-He (light green) and AFT (dark green) closure ages from the Colorado Plateau. (d) Histograms of closure ages across North America.

• To compare this inventory with our results we first converted reported closure ages into average denudation rates.

• We use a simple expression that relates surface and closure temperatures ( $T_s$, $T_c$ ), geothermal gradients ( $dT/dz$ ) and closure ages ( $a_c$ ) to calculate time-averaged denudation rate, where $T = (T_c - T_s)$.

$$\frac{dz}{dt} = \frac{T}{a_c(dT/dz)}$$

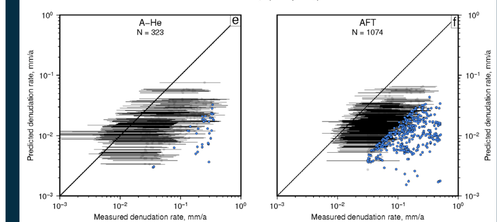

**Figure 13: Comparison of calculated and independent denudation rates.** (a) Comparison of denudation rates calculated using inverse model and from independent A-He closure ages. Error bars = range of measured denudation rates; blue points show where our calculated denudation rates are a factor of two or more lower than A-He estimates; note error bars have been omitted for clarity. (f) Comparison of calculated denudation rates and independent estimates from AFT closure ages.

## 7 Conclusions

1) Large compilations of geological data can be used to measure uplift and denudation rates at large length and timescales.

2) Inversion of drainage patterns can be used to 'fill-in' the gaps between geological observations of uplift and to investigate how uplift rates change through time.

3) From our measured and calculated uplift and denudation histories we can infer that sub-plate support has played a significant role in generating much of North America's landscape, especially at wavelengths greater than a few tens of kilometers.

**Figure 14: North American Landscape Evolution Model.** Four panels show Mesozoic to Cenozoic topographic evolution calculated using our parametrized forward model compared to coeval independent paleogeographic constraints. Red circles = magmatism from NAVDAT database; Blue circles = stratigraphic shoreline markers/marine fossil collections from the Paleobiology Database (Figure 6); light blue shading = maximum flooded surface from Smith et al., (1994) corrected using stratigraphic and biostratigraphic constraints.

## 8 References

[1] Galloway, W. E., T. L. Whiteaker, and P. Ganey-Curry (2011), History of Cenozoic North American drainage basin evolution, sediment yield, and accumulation in the Gulf of Mexico basin, Geosphere, 7(4), 938–973.

[2] Gleadow, A. J. W., and R. W. Brown (1999), Fission track thermochronology and the long-term denudational response to tectonics., Geomorphol. Glob. Tectonics, (May), 57–75.

[3] Poag, C. W., and W. D. Sevon (1989), A record of Appalachian denudation in postrift Mesozoic and Cenozoic sedimentary deposits of the U.S. Middle Atlantic continental margin, Geomorphology, 2(1-3), 119–157.

[4] Roberts, G. G., N. J. White, G. L. Martin-Brandis, and A. G. Crosby (2012a), An uplift history of the Colorado Plateau and its surroundings from inverse modeling of longitudinal river profiles, Tectonics, 31(4), 1–25.

[5] Rudge, J. F., G. G. Roberts, N. J. White, and C. N. Richardson (2015), Uplift histories of Africa and Australia from linear inverse modeling of drainage inventories, J. Geophys. Res. F Earth Surf., 120(5), 894–914.

[6] Salles, T. (2015), Badlands: A parallel basin and landscape dynamics model, SoftwareX, 5, 195–202.

[7] Schaeffer, A. J., and Lebedev, S. (2013), Global shear speed structure of the upper mantle and transition zone, Geophys. J. Int., 149, 417–449.

[1]Department of Earth Science and Engineering, Imperial College, London, UK.
[2]Bullard Laboratories, University of Cambridge, UK.